ACS APPLIED MATERIALS & INTERFACES

Applications of Polymer, Composite, and Coating Materials

A coreactant-free dual amplified electrochemiluminescent (ECL) biosensor based on conjugated polymer dots for the ultrasensitive detection of microRNA

Jinhua Luo, Qin Li, shihong Chen, and Ruo Yuan

ACS Appl. Mater. Interfaces, **Just Accepted Manuscript** • DOI: 10.1021/acsami.9b09339 • Publication Date (Web): 09 Jul 2019

A coreactant-free dual amplified electrochemiluminescent (ECL) biosensor based on conjugated polymer dots for the ultrasensitive detection of microRNA

Jin-Hua Luo[a], Qin Li[b], Shi-Hong Chen*[a], and Ruo Yuan[a]*

[a] Key Laboratory of Luminescent and Real-Time Analytical Chemistry (Southwest University), Ministry of Education, College of Chemistry and Chemical Engineering, Southwest University, Chongqing 400715, China.

[b] Gastroenterology, People's Hospital of Shapingba District of Chongqing, Chongqing 400030, China.

ABSTRACT

Generally, electrochemiluminescence (ECL) assays are performed in the presence of the coreactant. The addition of the coreactant in the detection solution would make the ECL system lack sufficient stability. In the case of dissolved oxygen as coreactant, the unknown concentration of dissolved O_2 would result in an inevitable error and the lack of reproducibility in detection. A coreactant-free ECL assay could overcome above shortcomings, thus is an ideal choice. In this work, a coreactant-free dual amplified electrochemiluminescent (ECL) strategy was constructed for ultra sensitively detecting of microRNA (miRNA). Here, target-catalyzed hairpin assembly and enzyme-triggered DNA walker recycling amplification were integrated to achieve the dual signal amplification. Carboxyl-functionalized poly[9,9-dioctylfluorenyl-2,7-diyl)-Co-1,4-benzo-{2,1'-3}-

thiadiazole)](PFBT-COOH) dots were used as luminophore, which displayed a prominent ECL performance without adding any coreactant and removing the dissolved O_2. As a result, the detection of miRNA was achieved, and the linear range was from 10 aM to 5 pM and the detection limit was low to 3.3 aM. Meanwhile, the practicability of our biosensor was investigated by analyzing the expression of miRNA in cell lysates. The PFBT-COOH dots provided a great platform for constructing coreactant-free ECL biosensor and expanded the application of conjugated polymer dots in clinic analysis.

KEYWORDS: Electrochemiluminescence, biosensor, PFBT-COOH, microRNA, coreactant-free

1. INTRODUCTION

MicroRNAs (miRNAs) are a kind of endogenetic, nonprotein-coding, short (typically about 19-25 nucleotides) and single-stranded RNAs[1-3], which have been certified to be significant regulators in several biological processes such as hematopoiesis[4], cell proliferation[5], and apoptosis[6]. Research evidences have indicated that the abnormal expression of miRNAs is related to the occurrence of various cancers[7]. Therefore, it is urgent to exploit a sensitive, highly specific and reliable assay for detecting miRNAs.

Electrochemiluminescence (ECL), integrating the chemiluminescence (CL)[8] and electrochemical technique[9,10], possesses high sensitivity, wide dynamic range, facility and good stability. It has been used widely in environmental analysis, biochemical

and clinical examination[11-13]. Generally, in order to obtain a high ECL signal intensity, the ECL assays were performed in the presence of coreactant. The most common way to use coreactant in ECL detection is to add it into testing solution. The addition of exogenous coreactant would affect the environment of the testing solution, and make the ECL system lack sufficient stability, thus resulting in a measurement error[14]. In order to avoid the defects from the addition of exogenous coreactant into testing solution, the following measures were adopted: (1) applying an enzyme to catalyze for in situ generating coreactant[15]; (2) immobilizing the coreactant on the surface of electrode[16]; (3) preparing self-enhanced complexes by integrating the luminophores and their coreactant in the same molecular structure or composite[17,18.] Although above methods indeed could improve the luminous stability and luminous efficiency of luminophores in ECL system, the complexity of the operation and the harsh use conditions of the enzyme limited their application. Additionally, utilizing dissolved O_2 as coreactant also could avoid the defects of the addition of exogenous coreactant[19-21], but the unknown concentration of dissolved O_2 would result in an inevitable errors and the lack of reproducibility in detection. Thus, it is very valuable to develop an ECL system with high ECL emission efficiency in the absence of any exogenous coreactant and dissolved O_2.

Recently, the conjugated polymers exhibits outstanding features such as high charge carrier mobility, facile surface functionalization, good photostability, thus have gained extensive attention[22,23].

Poly[9,9-dioctylfluorenyl-2,7-diyl)-Co-1,4-benzo-{2,1'-3}-thiadiazole)] (PFBT), as a typical conjugated polymer, has widespread applications in cellular abeling[24], fluorescent imaging and sensing[25,26]. However, the PFBT has been rarely used for the development of ECL sensing because of the poor water solubility. Ju's group designed a true-color ECL imaging strategy using PFBT polymer dots as the emitters for a multi-immunoassay of proteins[27]. This report pioneered the application of PFBT dots in ECL field, but tripropylamine was added as the coreactant of PFBT dots. As mentioned above, the addition of exogenous coreactant would make the ECL system lack stability. In our previous study, the poly-(styrene-co-maleicanhydride) (PSMA) was applied as the functional copolymer to prepare the carboxyl-functionalized poly(9,9-dioctylfluorenyl-2,7-diyl) (PFO) dots (Pdots), and an enough strong ECL signal was obtained firstly without adding any coreactant because of the increase of water solubility[28]. Nevertheless, because of the insufficient stability and film-forming of Pdots, the chitosan was used as an immobilization matrix. The non-conductive property of chitosan would obviously impede the ECL performance of Pdots. Fortunately, the PSMA functionalized PFBT (PFBT-COOH) dots not only exhibited a superior ECL property but also revealed an excellent film-forming ability. In the case of without adding any coreactant and removing the dissolved oxygen with N_2, the ECL strength of PFBT-COOH dots could reach 18,000 a.u., which was about 5 times higher than that of Pdots and 24 times higher than that of pure PFBT. Thus PFBT-COOH dots could act as a new ECL emitter with fantastic luminous efficiency.

The DNA walkers have drawn extensive attention because of the effective and accurate signal amplification[29,30]. As a consequence, utilizing PFBT-COOH dots as luminophore, a coreactant-free dual amplified ECL biosensor was constructed to sensitively detect miRNA-155 in collaboration with target-catalyzed hairpin assembly and enzyme-triggered bipedal DNA walker recycling amplification. As shown in Scheme 1, firstly, the PFBT-COOH dots were modified onto the electrode surface, which acted as the matrix for assembling DNA S1 to obtain a super strong ECL signal without adding any coreactant. Next, the black hole quencher (BHQ)-labeled DNA S2 (BHQ-S2) was introduced by hybridizing with S1. Herein, the ECL signal achieved a "signal-off" state due to the high quenching efficiency of BHQ. Finally, the bipedal DNA walkers produced via target-catalyzed hairpin assembly and Exonuclease III (Exo III) were incubated onto the electrode simultaneously. On the one hand, the BHQ-S2 was displaced by the bipedal DNA walker to be released from the surface of electrode. On the other hand, the Exo III digested the recessed 3' termini and blunt of double-stranded DNA[31], and made the DNA walker free to displace another BHQ-S2, achieving the DNA walker recycling processes. As expectedly, the ECL signal switched to "signal-on" state. Due to the integration of high luminous efficiency of PFBT-COOH dots, high quenching efficiency of BHQ as well as the dual amplified strategy, the proposed ECL "off−on" biosensor achieved the ultrasensitive detection of miRNA-155. Furthermore, the expression of miRNA-155 in cell lysates was analyzed to evaluate the practicability of the biosensor. Satisfactorily, the

PFBT-COOH dots provided a great platform for the construction of coreactant-free ECL biosensor. Meanwhile, the combination of PFBT-COOH dots and black hole quencher provided a new idea for determining miRNA-155 in clinic analysis.

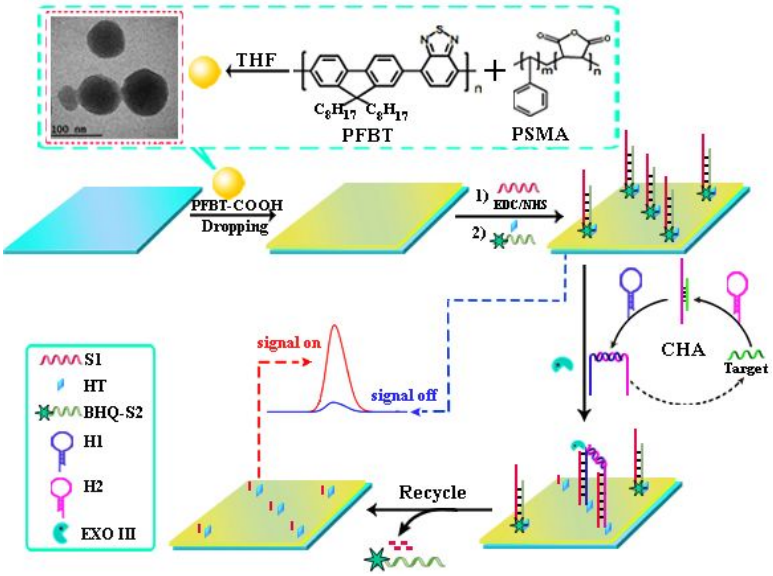

Scheme 1. Schematic illustration of the synthesis of PFBT-COOH dots and construction of biosensor

2. EXPERIMENTAL

2.1. Preparation of the PFBT-COOH Dots

Firstly, the stock solutions of PFBT and PSMA with a concentration of 1.0 mg/mL were prepared by dissolving them in THF, respectively. Then, 4.0 mL of the prepared PFBT and 800 μL of PSMA were mixed and sonicated to obtain the homogeneous solution. Subsequently, ultrapure water (10 mL) was injected into above solution and stirred overnight. Finally, partial vacuum evaporation was performed to remove THF from the solution and obtain PFBT-COOH dots.

2.2. Preparation of DNA Walkers (Secondary Target)

The DNA walkers were synthesized through the target-catalyzed hairpin assembly process. Firstly, the hairpins (H1 and H2) were treated by heating them at 90 °C for 5 min and slowly cooling down to room temperature prior to use. Then, target miRNA (10 μL), H1 (10 μM, 5 μL) and H2 (10 μM, 5 μL) were mixed. Afterwards， the mixed solution was incubated at 37℃ for 90 min to form DNA walkers

2.3. Construction of Biosensor

The assembly process of the biosensor is depicted in Scheme 1. Firstly, a glassy carbon electrode (GCE) with a diameter of 4.0 mm was pretreated, as reported in the reference[28]. Then, it was modified with 10 μL of PFBT-COOH dispersion. After dried, the modified electrode was immersed in cross-linking agent (0.02 g/mL of EDC and 0.01 g/mL of NHS) at room temperature for 30 min. Then, S1 (10 μL, 10 μM) was incubated onto the PFBT-COOH dots layer with active carboxyl groups at 4℃ overnight. After the nonspecific sites were blocked with HT (1.0 mM) for 40 min at room temperature, BHQ-S2 composite (10 μL, 10 μM) was incubated on the electrode for 2 h at 37℃. Subsequently, Exo Ⅲ (5 μL) and prepared DNA walker (10 μL) were cast onto the surface of decorated electrode. The ECL response of the modified electrodes was detected in 2.0 mL PBS (0.10 M, pH 7.4). During the ECL measurement, the following parameters were set, including the voltage of 800 V for photomultiplier tube (PMT), the amplifier series of 3 and the scan rate of 0.3 V/S.

3. RESULTS AND DISCUSSION

3.1. ECL Property of PFBT-COOH Dots

The ECL property of PFBT-COOH dots and pure PFBT modified electrodes was studied in PBS, respectively. As displayed in Fig. 1A, the PFBT/GCE displayed a weak ECL emission about 700 a.u. (the black curve). Nevertheless, the PFBT-COOH dots/GCE exhibited an extraordinarily improved ECL response about 18000 a.u. (the red curve), which was about 24 times higher than that of pure PFBT. The reasonable interpretation may be as follows. The modification of carboxyl groups could enhance the water solubility of polymer dots, and enhance the effective concentration of the luminophore, thus leading to an increase in ECL signal, as reported in our previous work[28].

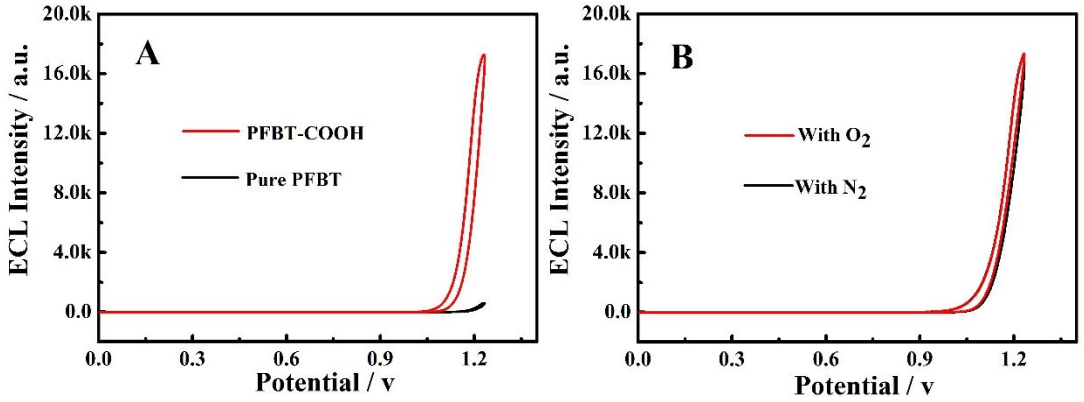

Fig. 1. The ECL response of (A) PFBT-COOH dots/GCE and PFBT/GCE, (B) PFBT-COOH dots/GCE with O_2 and with N_2 in PBS

3.2. Possible ECL Mechanism of PFBT-COOH Dots

In this work, we firstly explored whether the dissolved oxygen in solution served as the coreactant of PFBT-COOH dots. The ECL response of PFBT-COOH dots/GCE was measured in PBS with dissolved O_2 and deoxygenated with N_2, respectively. As

demonstrated in Fig. 1B, there was no significant distinction between the two curves, suggesting that the strong ECL emission of PFBT-COOH dots was not ascribed to the dissolved O_2.

Secondly, we investigated whether the reactive oxygen species (ROS) ($O_2^{\bullet-}$ and $OH^{\bullet}$) produced in the surface of electrode served as the intermediate to react with PFBT-COOH dots. In order to confirm it, L-cysteine was employed as the scavenger of $O_2^{\bullet-}$ and $OH^{\bullet}$. As well, the superoxide dismutase (SOD) was employed as the purifier to eliminate $O_2^{\bullet-}$. As seen from Fig. 2A and Fig. 2B, there was no significant difference in ECL response before and after treatment using L-cysteine and SOD, indicating that $O_2^{\bullet-}$ and $OH^{\bullet}$ did not serve as the intermediate to enhance the ECL signal of PFBT-COOH dots.

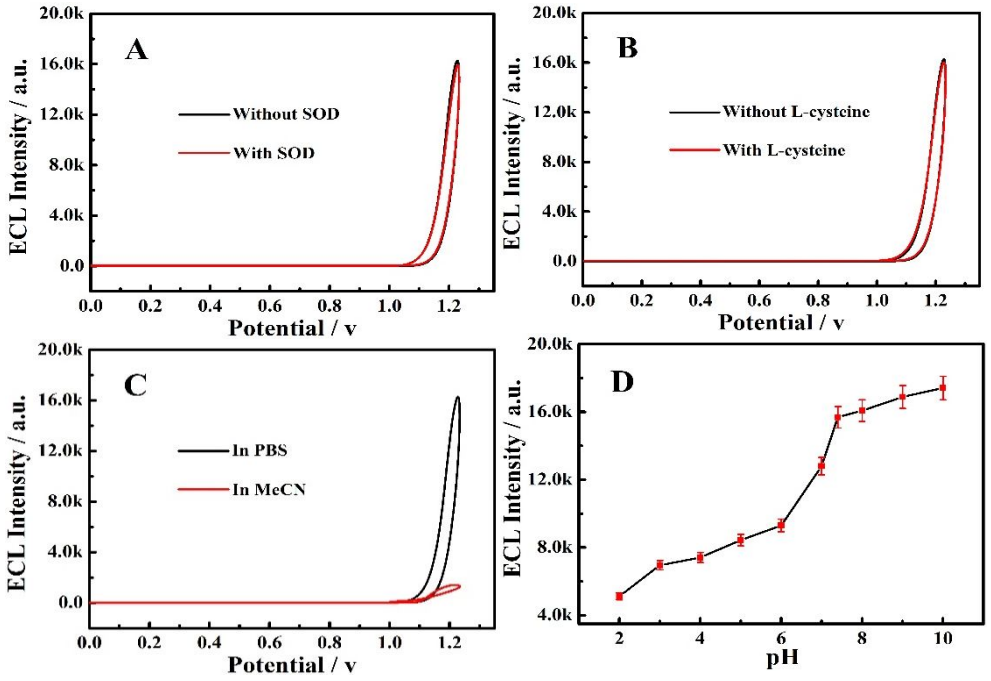

Fig. 2. ECL response of PFBT-COOH dots/GCE (A) without SOD (curve black) and with SOD (curve red) in PBS, (B) without L-cysteine (curve black) and with L-cysteine (curve red) in PBS,

(C) in PBS (curve black) and in MeCN (curve red) and (D) in PBS with different pH values

To explore the ECL mechanism of PFBT-COOH dots, we also compared the ECL behavior of PFBT-COOH dots/GCE in MeCN system and in PBS. As shown in Fig. 2C, in MeCN system, there was a weak ECL emission while a strong ECL emission was observed in PBS, indicating that the aqueous solution may play a key role. To testify whether the enhanced ECL emission was caused by the OH^- in PBS, the ECL behavior of PFBT-COOH dots/GCE in PBS solutions at different pH values was investigated. As expectedly, with pH values of PBS solution increasing from 2 to 10, the ECL response increased (Fig. 2D). Actually, when pH>10, the ECL intensity increased continuously (the data not shown here). Above facts indicted that the OH^- does play a vital role on the ECL emission of the PFBT-COOH dots. In fact, similar amplification effect of OH^- on the ECL emission has been observed in an organic ECL emitter[32]. The possible mechanism is speculated as Scheme 2. Firstly, PFBT-COOH was oxidized to produce the radical cation of PFBT-COOH ($PFBT\text{-}COOH^{+\bullet}$) on the surface of electrode. Then the proton of $PFBT\text{-}COOH^{+\bullet}$ was eliminated through the reaction between $PFBT\text{-}COOH^{+\bullet}$ and OH^- in PBS to give the reducing intermediate radical $PFBT\text{-}COOH^{\bullet}$. Finally, $PFBT\text{-}COOH^{\bullet}$ could reduce $PFBT\text{-}COOH^{+\bullet}$ to generate the excited-state PFBT-COOH*, thus yielding ECL emission.

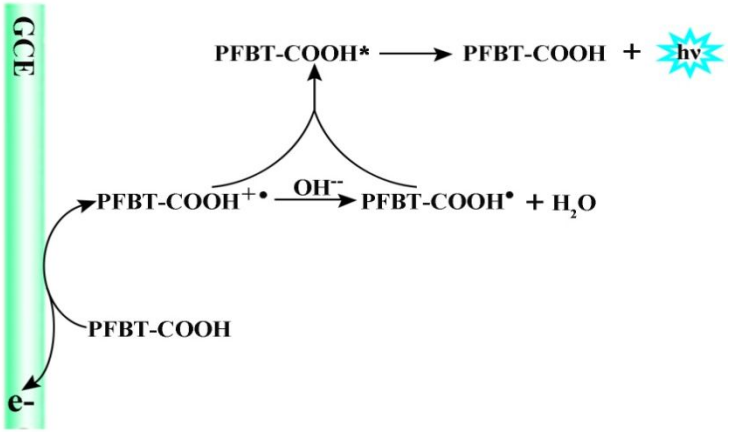

Scheme 2. Possible ECL mechanism of the PFBT-COOH dots

3.3. Characterization of ECL Biosensor and Optimization of Incubation Time of DNA Walker

The cyclic voltammograms (CVs) was measured in 5.0 mM $[Fe(CN)_6]^{3-/4-}$ to characterize the stepwise fabrication process of the biosensor. As seen from Fig. 3A, the bare GCE showed a couple of quasi-reversible redox peaks in CVs (curve a). For the electrode modified with PFBT-COOH dots , the redox current was declined (curve b) due to the hindrance of the thin film on the electrode surface for electron transfer. Since DNA could impede the electron transmission, a notable decreased redox current was detected after S1 was incubated onto the electrode (curve c). After the nonspecific binding sites were blocked with HT, the modified electrode displayed an increased redox current (curve d). When BHQ-S2 was introduced, the peak current slightly decreased (curve e). Then, the redox current increased obviously when the walker and Exo III were incubated on the electrode surface (curve f), because the BHQ-S2 was displaced by the bipedal DNA walker to be released from the electrode

surface. Simultaneously, the walker was free to displace another BHQ-S2 with the cleavage of the S1 assisted by the Exo III.

The electrochemical impedance spectroscopy (EIS) at each fabrication step was measured in 5.0 mM $[Fe(CN)_6]^{3-/4-}$ solution. Fig. 3B exhibits the corresponding results. As seen, a fairly small semicircle was observed at bare GCE (curve a), indicating a low electron-transfer resistance (R_{et}). The R_{et} of the PFBT-COOH dots modified electrode was increased (curve b). After introducing with S1, the R_{et} further increased (curves c). With the incubation of HT on the electrode, the R_{et} decreased (curve d). When BHQ-S2 was introduced, the R_{et} increased (curve e). Then, the R_{et} decreased obviously when the walker and Exo III were incubated on the electrode surface (curve f). The results of EIS characterization further suggested that our proposed ECL biosensor was constructed successfully.

Fig. 3C displays the ECL response in 0.10 M PBS (pH 7.4) of the stepwise fabrication process of the biosensor. As seen, no ECL response was observed at the bare GCE (curve a). Interestingly, PFBT-COOH dots/GCE presented a remarkable ECL signal with nearly 18000 a.u. in the case of coreactant-free (curve b), indicating a great ECL luminous efficiency of PFBT-COOH dots. After the electrode was incubated with S1 and further blocked with HT (curve c), the ECL response declined slightly. When BHQ-S2 was introduced (curve d), a distinctly decreased ECL signal was achieved because of the excellent ECL quenching effect of BHQ on PFBT-COOH dots. However, when the walker and Exo III were incubated onto the

electrode surface simultaneously (curve e), the numerous quencher BHQ was away from the electrode surface, thus the quenched ECL signal was recovered to 'on' state.

The loading amount of DNA track to the electrode and the density of DNA track on the electrode were investigated by cyclic voltammetry (CV)[33] and chronocoulometry (CC)[34]. The density of DNA track in this work was calculated as 8.13×10^{12} molecules cm^{-2}, as presented in *SI 1.5*, indicating a high loading of DNA track on the modified electrode.

Additionally, the effect of incubation time of DNA walker on the ECL emission of the modified electrode was investigated. As shown in Fig. 3D, with incubation time increasing from 10 min to 120 min, the ECL intensity increased. When incubation time exceeded 120 min, the intensity changed slowly, thus the optimal time of DNA walker was chosen as 120 min.

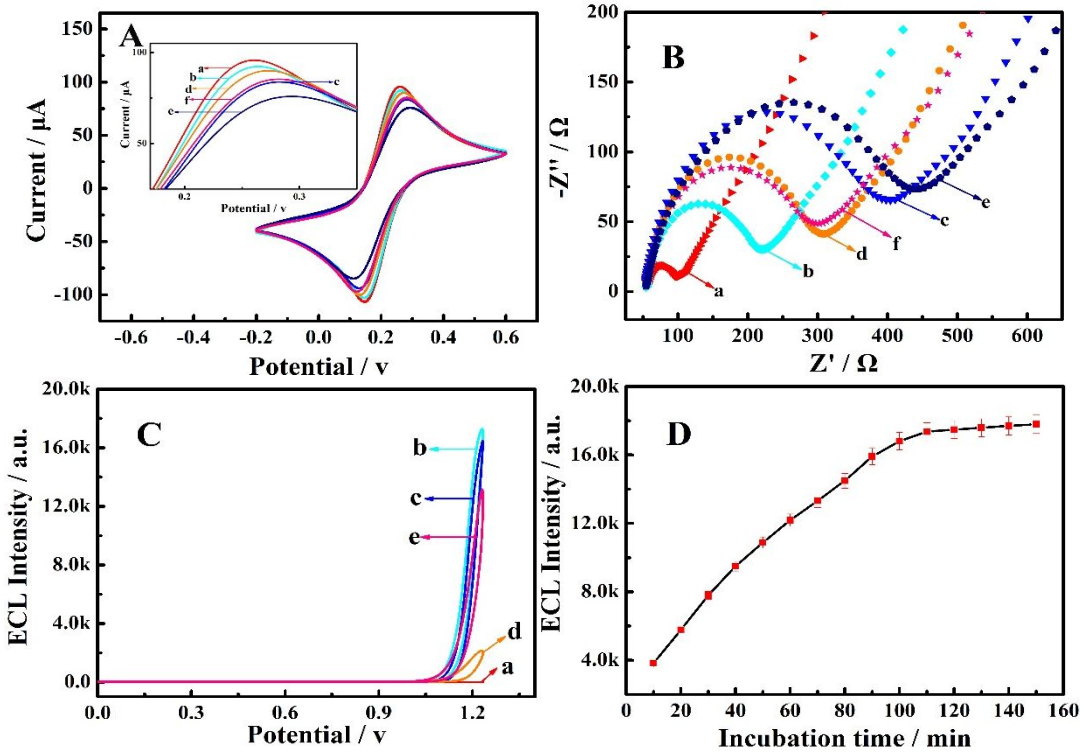

Fig. 3. (A) CV and (B) EIS characterization of the stepwise fabrications of the biosensor: (a) bare GCE, (b) PFBT-COOH dots/a, (c) S1/b, (d) HT/c, (e) BHQ-S2/d, (f) DNA walker/Exo Ⅲ/e; (C) ECL performance of the stepwise modified electrode: (a) bare GCE, (b) PFBT-COOH dots/a, (c) S1/HT/b, (d) BHQ-S2/c, (e) DNA walker/Exo Ⅲ/d; (D) ECL response in different incubation time of DNA walker

3.4. ECL Measurement of Biosensor

The quantitative measurements of the miRNA-155 were performed using the proposed ECL biosensor at optimal conditions with the "off−on" mode. Fig. 4A depicts the results. And the ECL response without target revealed a low ECL signal (curve a). Meanwhile, when the concentration of miRNA-155 increased from 10 aM to 5 pM, the anode ECL signal increased, and the evaluated detection limit is 3.3 aM (S/N = 3). As seen from Fig. 4B, the I_{ECL} exhibited a positive correlation with the logarithmic value of miRNA-155 concentration (lg*c*). Linear equation was $I = 45813.8 + 2573.6 \lg c$ with the square of the correlation coefficient of $R^2 = 0.9938$.

Besides, Table 1 lists the comparison of the prepared biosensor with other reported assays. As seen, the proposed biosensor behaved a higher sensitivity and a lower detection limit. It can be attributed to following reasons: (1) The PFBT-COOH dots possess a significant luminous efficiency; (2) The ECL-RET from excited PFBT-COOH dots to BHQ results in a high annihilation efficiency of BHQ on the ECL signal of PFBT-COOH dots (as presented in *SI 1.4*), thus giving a low

background signal,; (3) The target-catalyzed hairpin assembly and bipedal DNA walkers were integrated to achieve a dual amplification.

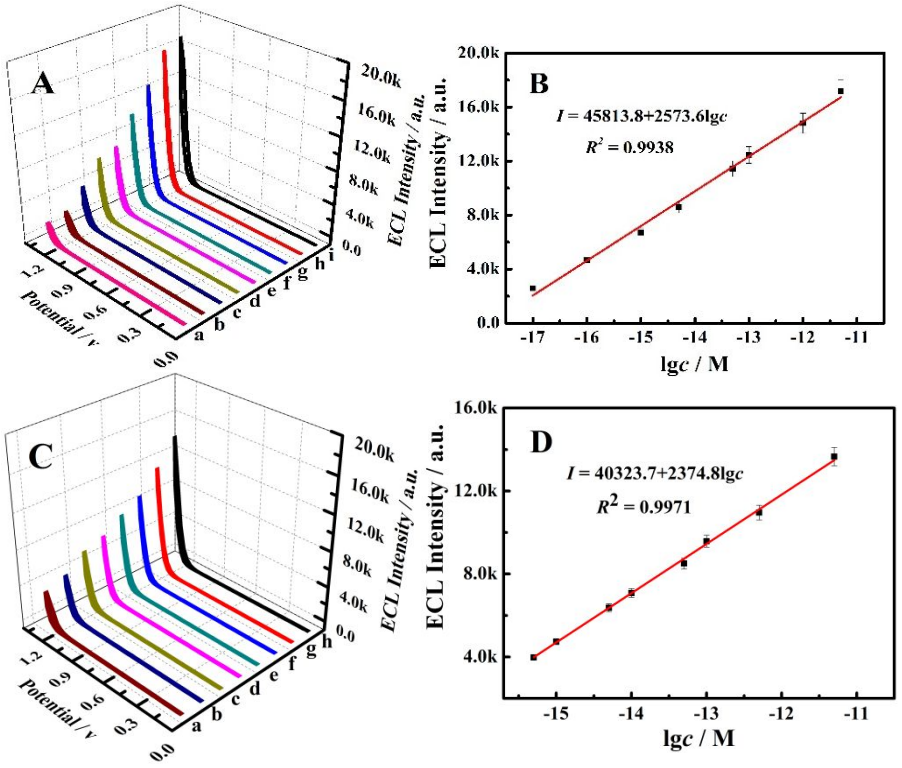

Fig. 4. (A) ECL response of the biosensor towards miRNA-155 with different concentrations: 0, 10 aM, 100 aM, 1 fM, 5 fM, 50 fM, 100 fM, 1 pM and 5 pM (from a−i); (C) ECL response of the modified electrode with DNA walker but without Exo Ⅲ towards miRNA-155 with different concentrations: 0.5 fM, 1 fM, 5 fM, 10 fM, 50 fM, 100 fM, 0.5 pM and 5 pM (from a−h); (B) and (D) The corresponding calibration curve for the ECL intensity *vs* the logarithm of miRNA-155 concentration

3.5. Comparison of ECL Response of Different Modified Electrodes

In order to testify that this system is a DNA walker rather than enzymatic cleavage, we tested the ECL response of BHQ-S2/HT/S1/PFBT-COOH dots/GCE in the case of with Exo Ⅲ alone, with DNA walker alone and with both DNA walker

and Exo Ⅲ, respectively. The results identified that this system is a DNA walker driven by Exo Ⅲ, as demonstrated in Fig. S5 (*SI 1.6*).

The ECL response of the BHQ-S2/HT/S1/PFBT-COOH dots/GCE towards miRNA-155 was examined in the case of with DNA walker but without Exo Ⅲ. As shown in Fig. 4C, anode ECL signal increased with the concentration of miRNA-155 increasing from 0.5 fM to 5 pM. Fig. 4D displayed the calibration curve for the ECL intensity *vs* the logarithm of miRNA-155 concentration and a detection limit of 0.17 fM was obtained (S/N = 3). Compared to the detection limit of 3.3 aM in the case of with Exo III for the two-step amplification, the detection limit in the absence of Exo III was about 50 times higher, indicating that the amplification strategy of the proposed biosensor performed an excellent amplified ability.

3.6. Selectivity and Stability of the miRNA Biosensor

Common short single-stranded RNAs including miRNA-21, miRNA-141, miRNA-126 and let-7a were employed as potential interfering substances to investigate the selectivity of the as-prepared biosensor. As depicted in Fig. 5A, compared to the blank, no obvious increase in ECL intensity was observed in the presence of 100 fM miRNA-21, miRNA-141, miRNA-126 and let-7a, respectively. Whereas, when the target miRNA-155 was tested at a low concentration (1 fM), the ECL intensity exhibited a significant increase. Besides, the mixture of 1 fM miRNA-155 and interference substances was also measured, and it was found that there was almost no difference in ECL signal intensity between the mixture and

miRNA-155 alone. The results indicated an outstanding specificity of the proposed biosensor.

The stability of our biosensor was evaluated in the presence of 10 fM miRNA-155. As seen from Fig. 5B, after consecutive cyclic scans for 16 cycles, the ECL response showed inconspicuous undulation with a relative standard deviation (RSD) of 0.04%, indicating a satisfying stability of the biosensor.

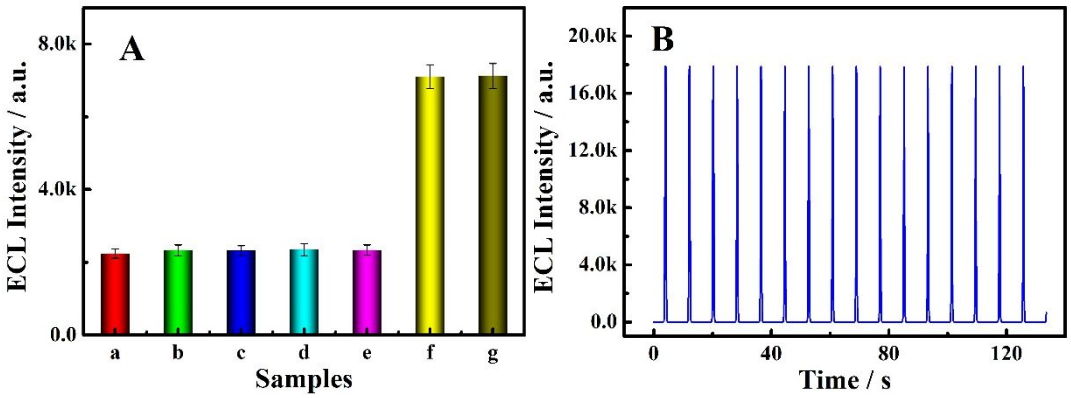

Fig. 5. (A) Selectivity of our biosensor with different RNAs: (a) blank, (b) miRNA-21(100 fM), (c) miRNA-141(100 fM), (d) miRNA-126(100 fM), (e) let-7a(100 fM), (f) miRNA-155(1 fM) and (g) mixture. (B) Stability of the elaborated biosensor

3.7. Practical Application of Biosensor

Practicability of the biosensor was estimated by investigating the expression of miRNA-155 in different cell lysates from human cervical cancer cell (Hela) and breast adenocarcinoma cell (MCF-7). As exhibited in Fig. 6, the blank displayed a weak ECL emission (a) and the ECL intensity increased with increasing the cell number from Hela. Meanwhile, when the concentration of MCF-7 increased from 10 to 10^4 cells, the ECL intensity increased obviously. The over expressed of

miRNA-155 in MCF-7 was consistent to the previous work[35]. The above consequences demonstrated that our proposed biosensor can offer a feasible and effective method for the detection of miRNAs.

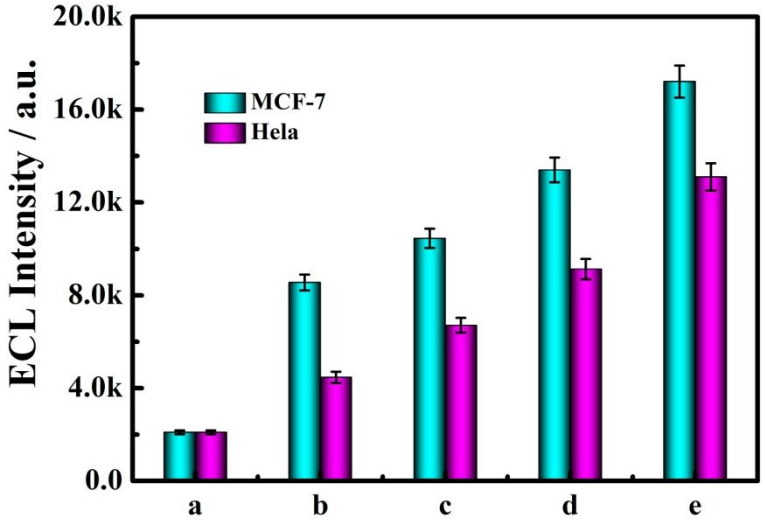

Fig. 6. ECL response towards miRNA-155 in cell lysates from Hela and MCF-7 with different numbers: (a) blank, (b) 10, (c) 10^2, (d) 10^3, (e) 10^4 cells

Table 1. Comparison of the prepared biosensor with other reported assays for miRNA detection

Determine method	Linear range	Detection limit	Reference
fluorescence	1 fM to 100 nM	1 fM	36
electrochemistry	5 fM to 5 pM	10 fM	37
ECL	1 fM to 50 pM	0.33 fM	38
ECL	100 aM to 1 nM	29.5 aM	39
ECL	10 aM to 5 pM	3.3 aM	This work

4. CONCLUSION

In this work, it was found that PFBT-COOH dots exhibited an unexceptionable ECL luminous efficiency without the addition of any coreactant and removing the dissolved O_2. More importantly, the black hole quencher (BHQ), as a common

quencher in fluorescence, could effectively quench the ECL intensity of PFBT-COOH dots. The combination of the high luminous efficiency of PFBT-COOH dots and the high quenching efficiency of BHQ provides a new, simple and sensitive ECL platform, and expands the application of polymer dots in bioanalysis. With PFBT-COOH dots as luminophore, we constructed a coreactant-free dual amplified ECL strategy for the ultrasensitive detection of miRNA in clinic analysis.

ASSOCIATED CONTENT

Supporting Information

Reagents and materials (SI 1.1), apparatus (SI 1.2), the comparison of ECL performance between PFBT-COOH dots and Pdots (SI 1.3), the quenching effect of BHQ on PFBT-COOH dots (SI 1.4), the determination of the density of DNA track on the electrode ECL (SI 1.5), comparison of ECL response of different modified electrodes (SI 1.6) and native polyacrylamide gel electrophoresis analysis of DNA walker (SI 1.7) were presented in Supporting Information.

AUTHOR INFORMATION

* **Corresponding authors:**

Tel: +86-23-65311326 Fax: +86-23-65311326.

E-mail address: 854761918@qq.com (Q. Li).

Tel: +86-23-68253172 Fax: +86-23-68253172.

E-mail address: cshong@swu.edu.cn (S.Chen).

Notes

The authors declare no competing financial interest.

ACKNOWLEDGMENTS

NNSF of China (21775122, 21775123, 21775124, 51473136, 21575116), and Natural Science Foundation of Chongqing City (cstc2018icyjAX0693), China supported this work.

REFERENCE

1. Hou, T.; Li, W.; Liu, X. J.; Li, F. Label-Free and Enzyme-Free Homogeneous Electrochemical Biosensing Strategy Based on Hybridization Chain Reaction: A Facile, Sensitive and Highly Specific MicroRNA Assay. *Anal. Chem.* **2015**, *87*, 11368−11374.

2. Bartel, D. P. MicroRNAs: Genomics, Biogenesis, Mechanism, and Function. *Cell*, **2004**, *116*, 281-97.

3. Chen, C. Z.; Li, L.; Lodish, H. F.; Bartel, D. P. MicroRNAs Modulate Hematopoietic Lineage Differentiation. *Science*, **2004**, *33*, 83−86.

4. Johnson, C. D.; Esquela-Kerscher, A.; Stefani, G.; Byrom, M.; Kelnar, K.; Ovcharenko, D.; Wilso in Human Cells. *Cancer Res.* **2007**, *67*, 7713−7722.

5. Chan, J. A.; Krichevsky , A. M.; Kosik, K. S. MicroRNA-21 Is an Antiapoptotic Factor in Human Glioblastoma Cells. *Cancer Res.* **2005**, *65*, 6029−6033.

6. Croce, C. M. MicroRNA Signatures in Human Ovarian Cancer. *Cancer Res.* **2007**, *67*, 8699-8707.

7. Lu, J.; Getz, G.; Miska, E. A.; Alvarez-Saavedra, E.; Lamb, J.; Peck, D.; Sweet-Cordero, A.; Ebert, B. L.; Mak, R. H.; Ferrando, A. A.; Downing, J. R.; Jacks, T.; Horvitz, H. R.; Golub, T. R. MicroRNA Expression Profiles Classify Human Cancers. *Nature*, **2005**, *435*, 834−838.

8. Miao, W. J. Electrogenerated Chemiluminescence and Its Biorelated Applications. *Chem. Rev.* **2008**, *108*, 2506−2553.

9. Wang, X. Y.; Chen, F.; Zhang, D. X.; Zhao, Y.; Wei, J.; Wang, L. H.; Song, S. P.; Fan, C. H.; Zhao, Y. X. Single Copy-Sensitive Electrochemical Assay for Circulating Methylated DNA in Clinical Samples with Ultrahigh Specificity Based on a Sequential Discrimination–Amplification Strategy. *Chem. Sci.* **2017**, *8*, 4764.

10. Chen, F.; Wang, X. Y.; Cao, X. W.; Zhao, Y. X. Accurate Electrochemistry Analysis of Circulating Methylated DNA from Clinical Plasma Based on Paired-End Tagging and Amplifications. *Anal. Chem.* **2017**, *89*, 10468−10473.

11. Zhou, Y.; Wang, H. J.; Zhang, H.; Chai, Y. Q.; Yuan, R. Programmable Modulation of Copper Nanoclusters Electrochemiluminescence via DNA Nanocranes for Ultrasensitive Detection of microRNA. *Anal. Chem.* **2018**, *90*, 3543−3549.

12. Ding, C. F.; Zhang, W.; Wang, W.; Chen, Y. Y.; Li, X. Q. Amplification Strategies Using Electrochemiluminescence Biosensors for the Detection of DNA, Bioactive Molecules and Cancer Biomarkers. *TrAC Trends in Anal. Chem.* **2015**, *65*, 137–150.

13. Zhang, Y.; Li, L.; Zhang, L. N.; Ge, S. G.; Yan, M.; Yu, J. H. In-Situ Synthesized Polypyrrole-Cellulose Conductive Networks for Potential-Tunable Foldable Power Paper. *Nano Energy*, **2017**, *31*, 174–182.

14. Wang, Y.; Lu, J.; Tang, L. H.; Chang, H. X.; Li, J. H. Graphene Oxide Amplified Electrogenerated Chemiluminescence of Quantum Dots and Its Selective Sensing for Glutathione from Thiol-Containing Compounds. *Anal. Chem.* **2009**, *81*, 9710–9715.

15. Gui, G. F.; Zhuo, Y.; Chai, Y. Q.; Xiang, Y.; Yuan, R. In Situ Generation of Self-Enhanced Luminophore by β-Lactamase Catalysis for Highly Sensitive Electrochemiluminescent Aptasensor. *Anal. Chem.* **2014**, *86*, 5873−5880.

16. Sun, B.; Qi, H. L.; Ma, F.; Gao, Q.; Zhang, C. X.; Miao, W. J. Double Covalent Coupling Method for the Fabrication of Highly Sensitive and Reusable Electrogenerated Chemiluminescence Sensors. *Anal. Chem.* **2010**, *82*, 5046.

17. Wang, H. J.; He, Y.; Chai, Y. Q.; Yuan, R. A super Intramolecular Self-Enhanced Electrochemiluminescence Immunosensor Based on Polymer Chains Grafted on Palladium Nanocages. *Nanoscale*, **2014**, *6*, 10316–10322.

18. Xiong, C. Y.; Liang, W. B.; Zheng, Y. N.; Zhuo, Y.; Chai, Y. Q.; Yuan, R. Ultrasensitive Assay for Telomerase Activity via Self-Enhanced Electrochemiluminescent Ruthenium Complex Doped Metal−Organic Frameworks with High Emission Efficiency. *Anal. Chem.* **2017**, *89*, 3222−3227.

19. Deng, S. Y.; Zhang, T. T.; Ji, X. B.; Wan, Y.; Xin, P.; Shan, D.; Zhang, X. J. Detection of Zinc Finger Protein (EGR1) Based on Electrogenerated Chemiluminescence from Singlet Oxygen Produced in a NanoclaySupported Porphyrin Environment. *Anal. Chem.* **2015**, *87*, 9155−9162.

20. Yao, C. G.; Song, H. X.; Wan, Y.; Ma, K. F.; Zheng, C. Y.; Cui, H. D.; Xin, P.; Ji, X. B. Deng, S. Y. Electro-Photodynamic Visualization of Singlet Oxygen Induced by Zinc Porphyrin Modified Microchip in Aqueous Media. *ACS Appl. Mater. Interfaces,* **2016**, *8*, 34833−34843.

21. Zheng, C. Y.; Sheng, Y. F.; Liu, Y.; Wan, Y.; Liu, G.; Zhang, X. T.; Yang, M.; Kang, K.; Liu, J. P.; Ma, K. F.; Deng, S. Y. Enhanced Electrochemiluminescent Brightness and Stability of Porphyrins by Supramolecular Pinning and Pinching for Sensitive Zinc Detection. *Anal. Bioanal. Chem.* **2019**, *19*, 4797-4806.

22. Chan, Y. H.; Wu, P. J. Semiconducting Polymer Nanoparticles as Fluorescent Probes for Biological Imaging and Sensing. *Part. Part. Syst. Charact.* **2015**, *32*, 11–28.

23. Wu, C. F.; Chiu, D. T. Highly Fluorescent Semiconducting Polymer Dots for Biology and Medicine. *Angew. Chem. Int. Ed.* **2013**, *52*, 3086 – 3109.

24. Wu, P. J.; Kuo, S. Y.; Huang, Y. C.; Chen, C. P.; Chan, Y. H. Polydiacetylene-Enclosed Near-Infrared Fluorescent Semiconducting Polymer Dots for Bioimaging and Sensing. *Anal. Chem*. **2014**, *86*, 4831−4839.

25. Chan, Y. H.; Jin, Y. H.; Wu, C. F.; Chiu, D. T. Copper(II) and Iron(II) Ion Sensing with Semiconducting Polymer Dots. *Chem. Commun.* **2011**, *47*, 2820–2822.

26. Wu, P. J.; Chen, J. L.; Chen, C. P.; Chan, Y. H. Photoactivated Ratiometric Copper(II) Ion Sensing with Semiconducting Polymer Dots. *Chem. Commun.* **2013**, *49*, 898.

27. Wang, N. N.; Feng, Y. Q.; Wang, Y. W.; Ju, H. X.; Yan, F. Electrochemiluminescent Imaging for Multi-immunoassay Sensitized by Dual DNA Amplification of Polymer Dot Signal. *Anal. Chem.* **2018**, *90*, 7708−7714.

28. Luo, J. H.; Cheng, D.; Li, P. X.; Yao, Y.; Chen, S. H.; Yuan, R.; Xu, W. J. An Electrochemiluminescent Sensor Based on Functionalized Conjugated Polymer Dots for the Ultrasensitive Detection of Cu^{2+}. *Chem. Commun.* **2018**, *54*, 2777.

29. Qu, X. M.; Zhu, D.; Yao, G. B.; Su, S.; Chao, J.; Liu, H. J.; Zuo, X. L.; Wang, L. H.; Shi, J. Y.; Wang, L. H.; Huang, W.; Pei, H.; Fan, C. H. An Exonuclease

III-Powered, On-Particle Stochastic DNA Walker. *Angew. Chem. Int. Ed.* **2017**, *56*, 1855 –1858.

30. Liu, W.; Chen, A. Y.; Li, S. K.; Peng, K. F.; Chai, Y. Q.; Yuan, R. Perylene Derivative/Luminol Nanocomposite as a Strong Electrochemiluminescence Emitter for Construction of an Ultrasensitive MicroRNA Biosensor. *Anal. Chem*. **2019**, *91*, 1516−1523.

31. Kow, Y. W.; Wallace, S. S. Exonuclease III Recognizes Urea Residues in Oxidized DNA. *Proc. Natl. Acad. Sci.* **1985**, *82*, 8355.

32. Ma, L.; Wu, N.; Liu, Y.; Ran, X. Q.; Xiao, D. B. Self-Electrochemiluminescence of Poly[9,9-bis(3‘-(N,N-Dimethyl-Amino) Propyl)-2,7-Fluorene]-alt-2,7-(9,9-Dioctylfluorene)] and Resonance Energy Transfer to Aluminum Tris(8-quinolinolate). *Electrochimica Acta*, **2019**, *297*, 826-832.

33.Singh, J.; Roychoudhury, A.; Srivastava,M.; Solanki, P. R.; Lee, D. W.; Lee, S. H.; Malhotra, B. D. A Dual Enzyme Functionalized Nanostructured Thulium Oxide Based Interface for Biomedical Application. *Nanoscale*, **2014**, *6*, 1195.

34. Zhang, J.; Song, S. P.; Wang, L. H.; Pan, D.; Fan, C. H. A Gold Nanoparticle-Based Chronocoulometric DNA Sensor for Amplified Detection of DNA. *Nature Protocols*, **2007**, *2*, 2888.

35. Lu Y J, Xiao J N, Lin H X, Bai Y L, Luo X B, Wang, Z G, Yang B F. A single anti-microRNA antisense oligodeoxyribonucleotide (AMO) targeting multiple microRNAs offers an improved approach for microRNA interference. *Nucleic Acids Res.*, **2009**, *37*, 1−10

36. Yin, B. C.; Liu, Y. Q.; Ye, B. C. Sensitive Detection of MicroRNA in Complex Biological Samples via Enzymatic Signal Amplification Using DNA Polymerase Coupled with Nicking Endonuclease. *Anal. Chem*. **2013**, *85*, 11487−11493.

37. Koo, K. M.; Carrascosa, L. G.; Shiddiky, M. J. A.; Trau, M. Poly(A) Extensions of MiRNAs for Amplification-Free Electrochemical Detection on Screen-Printed Gold Electrodes. *Anal. Chem*. **2016**, *88*, 2000−2005.

38. Zhang, P.; Lin, Z. F.; Zhuo, Y.; Yuan, R.; Chai, Y. Q. Dual microRNAs-Fueled DNA Nanogears: A Case of Regenerated Strategy for Multiple Electrochemiluminescence Detection of MicroRNAs with Single Luminophore. *Anal. Chem*. **2017**, *89*, 1338-1345.

39. Liu, J. L.; Tang, Z. L.; Zhang, J. Q.; Chai, Y. Q.; Zhuo, Y.; Yuan, R. Morphology-Controlled 9,10-Diphenylanthracene Nanoblocks as Electrochemiluminescence Emitters for MicroRNA Detection with One-Step DNA Walker Amplification. *Anal. Chem.* **2018**, *90*, 5298−5305.

For TOC only